GNA14 and *GNAQ* somatic mutations cause spinal and intracranial extra-axial cavernous hemangiomas

Graphical abstract

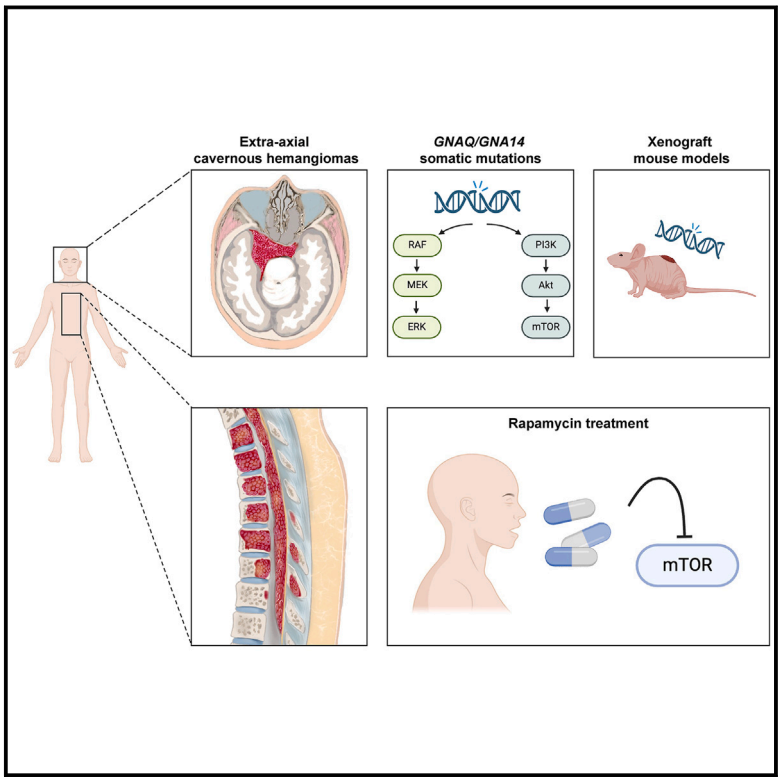

Authors

Jian Ren, Ziwei Cui, Chendan Jiang, ..., Mark L. Kahn, Hongqi Zhang, Tao Hong

Correspondence

xwzhanghq@163.com (H.Z.), 2030921@qq.com (T.H.)

Extra-axial cavernous hemangiomas (ECHs) are complex vascular lesions mainly found in the spine and cavernous sinus, and their genetic underpinnings remain incompletely understood. Here, we report somatic mutations of *GNA14*, *GNAQ*, and *GJA4* in ECH lesions. Furthermore, we present the utilization of rapamycin in treating an individual with *GNAQ* mutations.

Ren et al., 2024, The American Journal of Human Genetics *111*, 1–13
July 11, 2024
https://doi.org/10.1016/j.ajhg.2024.05.020

Please cite this article in press as: Ren et al., *GNA14* and *GNAQ* somatic mutations cause spinal and intracranial extra-axial cavernous hemangiomas, The American Journal of Human Genetics (2024), https://doi.org/10.1016/j.ajhg.2024.05.020

ARTICLE

GNA14 and *GNAQ* somatic mutations cause spinal and intracranial extra-axial cavernous hemangiomas

Jian Ren,[1,9] Ziwei Cui,[1,9] Chendan Jiang,[1,9] Leiming Wang,[2] Yunqian Guan,[3] Yeqing Ren,[1] Shikun Zhang,[1] Tianqi Tu,[1] Jiaxing Yu,[1] Ye Li,[1] Wanru Duan,[1] Jian Guan,[1] Kai Wang,[1] Hongdian Zhang,[4] Dong Xing,[5,6] Mark L. Kahn,[7] Hongqi Zhang,[1,*] and Tao Hong[1,8,*]

Summary

Extra-axial cavernous hemangiomas (ECHs) are complex vascular lesions mainly found in the spine and cavernous sinus. Their removal poses significant risk due to their vascularity and diffuse nature, and their genetic underpinnings remain incompletely understood. Our approach involved genetic analyses on 31 tissue samples of ECHs employing whole-exome sequencing and targeted deep sequencing. We explored downstream signaling pathways, gene expression changes, and resultant phenotypic shifts induced by these mutations, both *in vitro* and *in vivo*. In our cohort, 77.4% of samples had somatic missense variants in *GNA14*, *GNAQ*, or *GJA4*. Transcriptomic analysis highlighted significant pathway upregulation, with the *GNAQ* c.626A>G (p.Gln209Arg) mutation elevating PI3K-AKT-mTOR and angiogenesis-related pathways, while *GNA14* c.614A>T (p.Gln205Leu) mutation led to MAPK and angiogenesis-related pathway upregulation. Using a mouse xenograft model, we observed enlarged vessels from these mutations. Additionally, we initiated rapamycin treatment in a 14-year-old individual harboring the *GNAQ* c.626A>G (p.Gln209Arg) variant, resulting in gradual regression of cutaneous cavernous hemangiomas and improved motor strength, with minimal side effects. Understanding these mutations and their pathways provides a foundation for developing therapies for ECHs resistant to current therapies. Indeed, the administration of rapamycin in an individual within this study highlights the promise of targeted treatments in treating these complex lesions.

Introduction

Extra-axial cavernous hemangiomas (cavernous hemangiomas [MIM: 140850]) are benign vascular lesions characterized by dilated blood vessels predominantly observed in the spine and cavernous sinus.[1] Specifically, spinal extra-axial cavernous hemangiomas, including vertebral and epidural cavernous hemangiomas, are common vascular anomalies capable of causing symptoms due to neural compression.[2,3] In contrast, intracranial extra-axial cavernous hemangiomas primarily manifest within the cavernous sinus and occasionally in dural sinuses.[1,4]

Extra-axial cavernous hemangiomas and cavernous malformations (CMs [MIM: 116860]) intra-parenchymally within the brain and intramedullary spinal cord present differently in clinical symptoms, pathological characteristics, and radiotherapy sensitivity.[5] Regarding the limited understanding of the extra-axial cavernous hemangiomas, the terms of cavernous hemangiomas and cavernous malformations have often been used interchangeably, causing confusion among clinicians. The molecular basis of cerebral and intramedullary spinal cord CMs has been clearly delineated, involving activating *MAP3K3* (MIM: 602539) and *PIK3CA* (MIM: 171834) somatic mutations in sporadic CMs and bi-allelic loss-of-function (LoF) mutations in one of three cerebral cavernous malformation (CCM)-associated genes: *KRIT1* (MIM: 604214), *CCM2* (MIM: 607929), and *PDCD10* (MIM: 609118) in familial CMs.[6–10] Recent discoveries have identified *GJA4* (MIM: 121012) somatic mutations in orbital cavernous venous malformations (MIM: 600195) and intracranial extra-axial cavernous hemangiomas.[11,12] However, the causative factors behind spinal and intracranial extra-axial cavernous hemangiomas (ECHs) remain elusive.

We formulated the hypothesis that ECHs, encompassing vertebral, epidural, and cavernous sinus cavernous hemangiomas, may stem from somatic mutations in the vasculature. To test this hypothesis, we conducted comprehensive whole-exome sequencing (WES) and targeted deep sequencing of affected tissues. Our findings reveal a substantial percentage (77.4%) of somatic *GNA14* (MIM: 604397), *GNAQ* (MIM: 600998), and *GJA4* activating mutations within tissue samples of spinal and intracranial extra-axial cavernous hemangiomas ($n = 31$). To further explore the implications of these mutations, we established xenograft models by subcutaneously implanting *GNAQ* c.626A>G (p.Gln209Arg) and *GNA14* c.614A>T (p.Gln205Leu) endothelial cells (ECs) into immunodeficient mice, resulting in the formation of

[1]Department of Neurosurgery, Xuanwu Hospital, Capital Medical University, China International Neuroscience Institute, National Center for Neurological Disorders, Beijing, China; [2]Department of Pathology, Xuanwu Hospital, Capital Medical University, Beijing, China; [3]Cell Therapy Center, Beijing Institute of Geriatrics, Xuanwu Hospital Capital Medical University, National Clinical Research Center for Geriatric Diseases, and Key Laboratory of Neurodegenerative Diseases, Ministry of Education, Beijing, China; [4]Department of Neurosurgery, The Seventh Medical Center of PLA General Hospital, Beijing, China; [5]Biomedical Pioneering Innovation Center (BIOPIC), School of Life Sciences, Peking University, Beijing, China; [6]Beijing Advanced Innovation Center for Genomics (ICG), Peking University, Beijing, China; [7]Department of Medicine and Cardiovascular Institute, University of Pennsylvania, Philadelphia, PA, USA; [8]Department of Neurosurgery, Xiongan Xuanwu Hospital, Xiong'an New Area, China
[9]These authors contributed equally
*Correspondence: xwzhanghq@163.com (H.Z.), 2030921@qq.com (T.H.)
https://doi.org/10.1016/j.ajhg.2024.05.020.

Please cite this article in press as: Ren et al., *GNA14* and *GNAQ* somatic mutations cause spinal and intracranial extra-axial cavernous hemangiomas, The American Journal of Human Genetics (2024), https://doi.org/10.1016/j.ajhg.2024.05.020

enlarged blood vessels. Recognizing the promise of rapamycin as a potential agent for targeted pharmacologic management of vascular malformations, particularly its demonstrated benefits in *GNAQ* mutant Sturge-Weber syndrome (MIM: 185300),[13] we embarked on an investigation into its therapeutic potential for individuals afflicted with *GNAQ* mutant extra-axial cavernous hemangiomas.

Subjects and methods

Samples from human subjects

Between March 2007 and January 2023, a total of 43 consecutive individuals diagnosed with extra-axial cavernous hemangiomas underwent surgical resection of these lesions at the Department of Neurosurgery, Xuanwu Hospital, Capital Medical University. Tissue samples were successfully obtained from 31 individuals following surgical resection, including 28 with spinal cavernous hemangiomas and 3 with cavernous sinus hemangiomas (Table S1). The protocol was approved by the Ethics Committee of Xuanwu Hospital of Capital Medical University (approval number 2019-044) and was conducted in strict accordance with the ethical standards outlined in the 1964 Declaration of Helsinki. Written informed consent was obtained from all study participants.

Genetic analysis

We began our investigation by performing WES on a collection of 8 paraffin-embedded samples and 3 fresh-frozen tissue samples of extra-axial cavernous hemangiomas derived from 11 individuals. Furthermore, we incorporated 3 samples of associated cutaneous cavernous hemangiomas, 1 sample of muscle vascular lesion, and 1 sample of cutaneous wart lesion, all procured from a subset of these individuals. The tissue samples were sent to the sequencing facility of Nanjing Geneseeq Biotechnology Inc. for NGS analyses. Commercially available DNeasy Blood and Tissue Kit (Qiagen) with established protocols were used to isolate genomic DNA for whole-exome sequencing and downstream analyses. 1–2 μg genomic DNA for each sample was processed through fragmenting to 300–350 bp, end-repairing, A-tailing, and adaptor ligation using the Covaris M220 sonication system and KAPA Hyper Prep Kit (KAPA Biosystems, KK8504), followed by size selection and purification using Agencourt AMPure XP beads (Beckman Coulter). Libraries were amplified by PCR and purified using Agencourt AMPure XP beads. NanoDropTM 2000 (Thermo Fisher Scientific) for A260/280 and A260/230 ratios was used for sample quality control, Bioanalyzer 2100 with High Sensitivity DNA kit (Agilent Technologies, 5067-4627) was used for size distribution and Qubit 3.0 dsDNA HS Assays (Life Technology) was used for sample and library quantification. All of the procedures were according to the manufacturer's recommended protocols. xGen Exome Research Panel v.1.0 (Integrated DNA Technologies) was used for hybridization capture. Manufacturer's recommended protocol was followed. After target enrichment, the libraries were quantified by qPCR using KAPA Library Quantification Kit (KAPA Biosystems). Sequencing was performed on HiSeq4000 NGS platforms (Illumina) with paired-end 150 bp sequencing chemistry according to the manufacturer's instructions.

In order to corroborate the findings of the whole-exome sequencing, we performed targeted deep sequencing on genomic DNA extracted from an additional 20 paraffin-embedded samples of extra-axial cavernous hemangiomas. The targeted panel used for sequencing these cavernous hemangiomas encompasses 77 genes, which include *GNAQ*, *GNA14*, *GJA4*, *MAP3K3*, *PIK3CA*, *AKT1*, *KRIT1*, *CCM2*, and *PDCD10*. We targeted a sequencing depth of 1,000× for the tissue samples. Additionally, as a control group, we incorporated 75 samples of spinal cord intramedullary cavernous malformations and subjected them to whole-exome sequencing.

The targeted panel was customized by our team and iGeneTech Bioscience. The DNA was extracted with BunnyMag FFPE DNA Isolation Kit (BunnyTeeth Technology, TQ02BT). The quantity of extracted DNA was measured with Qubit 3.0 dsDNA HS Assays (Life Technology). A minimum of 50 ng genomic DNA were permitted to perform library preparation. The genomic DNA was fragmented mechanically to 150–250 bp segments with IGT Fast Library Prep Kit v.2.0. IGT Adapter & UDI Primer 1–96 (for Illumina, plate) was used to perform end-repairing, A-tailing, and adaptor ligation. The products were hybridized to biotin-labelled probes of the customized TargetSeq Target Probes T725V2 (iGeneTech Bioscience). Then, streptavidin-coated magnetic beads were used for specific capture of library fragments with targeted sequences (TargetSeq One Hyb & Wash Kit v.2.0 with Eco Universal Blocking Oligo [for Illumina], C10832 and TargetSeq Cap Beads & Nuclease-Free Water, C10422, iGeneTech Bioscience). The library whose Qubit concentration is larger than 25 ng/μL was regarded as qualified. Qsep 100 was also applied to ensure the peak of the size distribution was located within 220–450 bp. The sequencing was done with Illunima NovaSeq 6000 under PE150 mode, with a data amount target of 1G.

Bioinfomatic processing

For our WES samples, demultiplexing was carried out using bcl2fastq v.2.16.0.10 (Illumina). Adaptor nucleotides and low-quality base cells were removed by Trimmomatics.[14] Paired-end sequencing reads were aligned to the human reference genome hg19 (Genome Reference Consortium Human ref. 37, GRCh37) using Burrows-Wheeler Aligner v.0.7.12 (BWA-MEM).[15] Samtools v.1.6 was used to sort and index the aligned bam file.[16] The bam file was further processed for PCR-duplicate removal by Picard v.1.119 (https://broadinstitute.github.io/picard/) and for base recalibration and indel realignment by the Genome Analysis Toolkit v.3.6 (GATK).[17] MuTect somatic mode with default parameters was used for single nucleotide variant (SNV) identification.[18] SNVs displaying 41% population frequency within the 1000 Genomes project and dbSNP were also excluded.[19,20] Small insertions and deletions (indels) were detected using Scalpel.[21] Identified SNVs and indels were annotated with ANNOVAR[22] and manually reviewed on Integrative Genomics Viewer (IGV, https://igv.org/).

The quality of panel sequencing was measured by FastQC (v.0.12.1, https://www.bioinformatics.babraham.ac.uk/projects/fastqc/) and multiqc v.1.17.[23] Adapters were removed by Trimmomaticv 0.39.[14] BWA-MEM v.0.7.17 was used to map the reference genome and samtools v.1.12 was used for format conversion and indexing.[15,16] Our reference genome was hg19 (Genome Reference Consortium Human ref. 37, GRCh37). Base recalibration and duplicates removal were finished with GATK v.4.2.6.1.[17] The panel coverage was further measured with bamdst (https://github.com/shiquan/bamdst). The variation calling was done with VarScan v.2.4.3 and GATK.[17,24] The variants was annotated with ANNOVAR.[22] Variants with high population frequency, non-functional region were filtered.[19,20,25]

For RNA-seq, the genome of human genome version of hg38 (Genome Reference Consortium Human ref. 38, GRCh38) was

used as reference. The sequencing quality was assessed with FastQC and then low-quality data were filtered using NGSQC v.2.3.3.[26] The clean reads were then aligned to the reference genome using HISAT2 v.2.1.0 with default parameters.[27] The processed reads from each sample were aligned using HISAT2 against the reference genome. The expression analyses were performed with StringTie v.1.3.3b.[28] DESeq v.1.28.0 was used to analyze the DEGs between samples.[29] Thousands of independent statistical hypothesis testing was conducted on DEGs, separately. Then a p value was obtained, which was corrected by FDR method. Corrected p value (q-value) was calculated by correcting using BH method. p value or q-value were used to conduct significance analysis. Parameters for classifying significantly DEGs are $\geq$2-fold differences (log2FC $\geq$ 1, FC: the fold change of expressions) in the transcript abundance and $p \leq 0.05$. The annotation of the DEGs were performed based on the information obtained from the databases of ENSEMBL, NCBI, Uniprot, GO, and KEGG.

Cell culture and transfection

Human umbilical vein endothelial cells (HUVECs) were cultured on attachment factor-coated dishes and maintained in Endothelial Cell Medium (Sciencells) supplemented with 10% FBS (Sigma Aldrich). The HUVECs were generously provided by Shanghai East Hospital. Furthermore, human retinal pigment epithelial cells (h-RPEs) were cultured under similar conditions on attachment factor-coated dishes and fed with Dulbecco's Modified Eagle Medium (Gibco) supplemented with 10% FBS (Sigma Aldrich), provided by Sciencells. Lentiviruses carrying *GNAQ* c.626A>G, *GNAQ* WT, *GNA14* c.614A>T, *GNA14* WT, or empty vector constructs were generated by OBiO Tech (Shanghai, China). HUVECs were transfected with a transfection concentration of MOI = 10 following the manufacturer's guidelines. Transfected HUVECs were subsequently incubated at 37°C and 5% CO_2 in a humidified incubator for 16–24 h before being collected for further experiments. The sequences of the lentiviruses are detailed in Table S2.

Cell tube formation

To assess tube formation, a 96-well cell culture plate (Costa) was coated with 50 μL/well (equivalent to 50 μL/cm^2) of Matrigel Basement Membrane Matrix (CORNING, #356237) and incubated for 30 min at 37°C. After 48 h post-transfection, cells were digested, and cell suspensions (2×10^4 counts/well) were added to the plate, followed by incubation at 37°C with 5% CO_2 for 12 h. The total length of the tube network was quantified at a 40× magnification using a Retiga 1300 camera and a Nikon microscope (model TE2000-U).

RNA sequencing

Total RNA was meticulously extracted from HUVECs infected with lentiviruses expressing *GNAQ* c.626A>G, *GNAQ* WT, *GNA14* c.614A>T, *GNA14* WT, or empty vector using Trizol (Invitrogen). The quality of the RNA was diligently assessed using an Agilent 2100 BioAnalyzer (Agilent Technologies) and the Qubit Fluorometer (Invitrogen). Only total RNA samples meeting the stringent criteria of RNA integrity number (RIN) > 7.0 and a 28S:18S ratio >1.8 were deemed suitable for subsequent experiments. RNA-seq libraries were meticulously generated and subsequently sequenced by CapitalBio Technology. Notably, each of the triplicate samples from all assays underwent independent library construction, sequencing, and analysis. To construct the libraries for sequencing, the NEB Next Ultra RNA Library Prep Kit for Illumina (NEB) was employed. Furthermore, the NEB Next Poly(A) mRNA Magnetic Isolation Module (NEB) kit facilitated the enrichment of poly(A)-tailed mRNA molecules from 1 μg of total RNA. The mRNA was then judiciously fragmented into approximately 200 base pair fragments. Subsequently, the first-strand cDNA was synthesized from the mRNA fragments utilizing reverse transcriptase and random hexamer primers, followed by the synthesis of the second-strand cDNA employing DNA polymerase I and RNaseH. To complete the process, the end of the cDNA fragment was subjected to an end-repair process that included the addition of a single "A" base, followed by adapter ligation. The resulting products underwent purification and enrichment through polymerase chain reaction (PCR) amplification to augment the library DNA. The final libraries were meticulously quantified employing the KAPA Library Quantification kit (KAPA Biosystems) and an Agilent 2100 Bioanalyzer. Following quantitative reverse transcription-polymerase chain reaction (RT-qPCR) validation, the libraries were subjected to paired-end sequencing with a pair-end reading length of 150 base pairs on an Illumina NovaSeq sequencer (Illumina). The annotation of the DEGs (differentially expressed genes) was meticulously carried out based on the information sourced from the ENSEMBL, NCBI, UniProt, GO, and KEGG databases. Comparative data analysis was conducted by integrating self-test samples (GNAQ p.Gln209Arg and GNAQ WT) with RNA-sequencing data (GNAQ p.Gln209Arg, GNAQ p.Gln209Leu, GNAQ p.Arg183Gln, and GNAQ WT) from the GEO data repository (GEO: GSE199978) (http://www.ncbi.nlm.nih.gov/geo/),[30] following the removal of batch effects with ComBat algorithm.[31] The DEG method was limma.[32]

Western blotting

Proteins were carefully extracted from HUVECs infected with lentiviruses carrying *GNAQ* c.626A>G, *GNAQ* WT, *GNA14* c.614A>T, *GNA14* WT, or empty vector. Subsequent to cell lysis, protein analysis was performed through western blotting using established protocols. The following antibodies were employed: Gα(q) (CST, 14373, 1:1,000, rabbit); Angiopoietin-2 (R&D Systems, AF6231, goat); AKT (pan) (CST, 2920, 1:1,000, mouse); Phospho-AKT(Ser473) (CST, 4060, 1:1,000, rabbit); ERK 1/2 (Proteintech, 11257-1-AP, 1:2,000, rabbit); Phospho-ERK1/2 (Thr202/Tyr204) (Proteintech, 28733-1-AP, 1:1,000, rabbit); GAPDH (CST, 2118, 1:2,000, rabbit); anti-rabbit IgG (CST, HRP-linked Antibody #7074, 1:3,000, rabbit); anti-mouse IgG (CST, HRP-linked Antibody #7076, 1:3,000, mouse); and anti-Goat IgG (ZSGB-BIO, ZB-2306, 1:3,000).

Histological staining and immunohistochemistry

Tissue samples were collected, and sections (6 μm thick) were prepared after embedding in paraffin. These sections were then stained with hematoxylin and eosin (H&E), as well as antibodies against CD31 (Abcam, # [JC/70A] ab9498,1:200) and Ki67 (ZSGB-Bio, #ZM-0166, 1:200) following a standard protocol. Imaging of the stained sections was conducted using a VS120 Virtual Slide Microscope (Olympus).

Immunofluorescence

Frozen sections of subcutaneous implants from nude mice with different groups were immunofluorescent stained following a standard protocol. Briefly, sections were incubated with anti-ANGPT2 (R&D Systems, #AF623, 1:200) and anti-CD31 antibodies (Abcam, # [JC/70A] ab9498, 1:200) 3 days 4°C, followed by

incubation with second antibodies 2 h at room temperature, and then mounted with fluorescent mounting medium with DAPI (ZSGB-Bio, #ZLI-9557) and analyzed using a confocal laser-scanning microscope (Nikon AXR laser scanning microscope). Sections of each anti-human CD31-positive implant were analyzed and evaluated by immunofluorescence staining, with 3–4 fields of view selected from each specimen. Quantitative measurements were performed for each group using Fiji.[33]

Xenograft model for cavernous hemangiomas

For the creation of an *in vivo* murine model simulating human blood vessel formation, we combined 1.5×10^6 HUVECs producing GNAQ p.Gln209Arg, GNAQ WT, GNA14 p.Gln205Leu, or GNA14 WT along with 1.5×10^6 human retinal pigment epithelial cells (h-RPEs). The main role of h-RPEs is to provide support and nutrition to the blood vessels formed in the implants. This cellular mixture was suspended in 300 μL of Matrigel (Corning) and then subcutaneously injected into anesthetized 5-week-old male athymic BALB-nude mice. The selection of male nude mice was based on their docile nature and ease of handling compared to female counterparts, thereby enhancing overall safety during animal care and experimentation. Each experimental group consisted of $n = 5$ mice. After a 12-day period, the mice were humanely euthanized, and the implants were carefully excised for subsequent analysis. The experimental procedures involving mice in this study were approved by the Animal Experimental Ethical Inspection in Xuanwu Hospital of Capital Medical University.

Rapamycin treatment for one person

A 14-year-old female diagnosed with *GNAQ* c.626A>G (GenBank: NM_002072.5; p.Gln209Arg) mutant spinal epidural cavernous hemangiomas and associated cutaneous lesions received a treatment recommendation involving oral administration of rapamycin at a dosage of 1.5 mg per day. Dosage adjustments were made based on monthly serum levels of rapamycin, with a target range of 4–12 ng/mL. Throughout the course of treatment, spanning one year, spinal MRI scans and photographs of cutaneous lesions were performed every three months. Any side effects observed during treatment were meticulously recorded. The protocol of the rapamycin treatment was approved by the Ethics Committee of Xuanwu Hospital of Capital Medical University (approval number: 2019-071) and was conducted in strict accordance with the ethical standards outlined in the 1964 Declaration of Helsinki. Written informed consent was obtained from the affected individual and her guardian.

Statistical analysis

Our statistical analysis encompassed the utilization of Fisher's exact test or Pearson's χ^2 test (with or without Yates continuity correction) for categorical variables and Student's t test for continuous variables. All statistical analyses were conducted under the guidance of an epidemiologist utilizing SPSS software (v.25, IBM Corp.). All p values were calculated as 2-sided, and statistical significance was defined as a p value less than 0.05.

Result

Detection of somatic *GNAQ* and *GNA14* mutations

Among the 31 tissue samples obtained from extra-axial cavernous hemangiomas in our study, we identified somatic missense variants in *GNA14*, *GNAQ*, or *GJA4* in 24 samples, accounting for 77.4% of cases (Figure 1). Of these 24 samples, 14 exhibited a *GNA14* missense variant (GenBank: NM_004297.4; c.614A>T [p.Gln205Leu]) with variant frequencies ranging from 7.4% to 27.0%. This group included 10 cases of spinal pure epidural cavernous hemangiomas, 3 cases of vertebral epidural cavernous hemangiomas, and 1 case of cavernous sinus hemangiomas. Nine extra-axial cavernous hemangiomas exhibited somatic mutations in *GNAQ*. Specifically, we identified 7 cases of vertebral epidural cavernous hemangiomas and 2 cases of spinal pure epidural cavernous hemangiomas with *GNAQ* mutations. These mutations included *GNAQ* (GenBank: NM_002072.5; c.627A>C [p.Gln209His]) in 4 cases, *GNAQ* (GenBank: NM_002072.5; c.626A>G [p.Gln209Arg]) in 3 cases, *GNAQ* (GenBank: NM_002072.5; c.626A>T [p.Gln209Leu]) in 1 case, and *GNAQ* (GenBank: NM_002072.5; c.548G>A [p.Arg183Gln]) in 1 case. Variant frequencies for *GNAQ* somatic mutations ranged from 2.4% to 17.3%. In addition, we identified a *GJA4* somatic mutation (GenBank: NM_002060.3; c.121G>T [p.Gly41Cys]) in 1 case of cavernous sinus hemangiomas, with a variant frequency of 16.0%. Notably, in these samples of cavernous hemangiomas, we identified that the mutations in *GNAQ*, *GNA14*, and *GJA4* were mutually exclusive. None of the individuals have a family history of cavernous hemangiomas, and the variant frequency indicated that all the individuals displayed a sporadic form with somatic mutations.

Moreover, of the 3 individuals diagnosed with *GNAQ* mutant spinal cavernous hemangiomas, whole-exome sequencing of associated cutaneous cavernous hemangiomas, associated paravertebral muscle vascular lesion, and cutaneous wart lesion in these 3 individuals revealed identical *GNAQ* mutations as observed in the epidural lesions (Table S1). No pathological mutations in *GNAQ*, *GNA14*, or *GJA4* were found in the 75 control samples obtained from spinal cord cavernous malformations.

Clinicopathological features

In order to facilitate a comprehensive comparison of clinicopathological features between extra-axial cavernous hemangiomas carrying *GNAQ* or *GNA14* mutations and spinal cord cavernous malformations characterized by *CCM1* germline mutations, or *MAP3K3* and *PIK3CA* somatic mutations, we conducted H&E staining, CD31, and Ki67 immunohistochemical staining on paraffin-embedded samples. Histologically, both spinal epidural cavernous hemangiomas and cavernous sinus hemangiomas exhibited similar pathological features, characterized by widely dilated thin-walled vessels lined by a single layer of CD31-positive ECs, interspersed among adipocytes, indicative of cavernous hemangiomas (Figure 2). In contrast, when compared to spinal cord intramedullary cavernous malformations, extra-axial cavernous hemangiomas lacked obvious hemosiderin deposits. Ki67 staining revealed rare occurrences of $Ki67^+$ ECs in both extra-axial cavernous hemangiomas and spinal cord cavernous malformations.

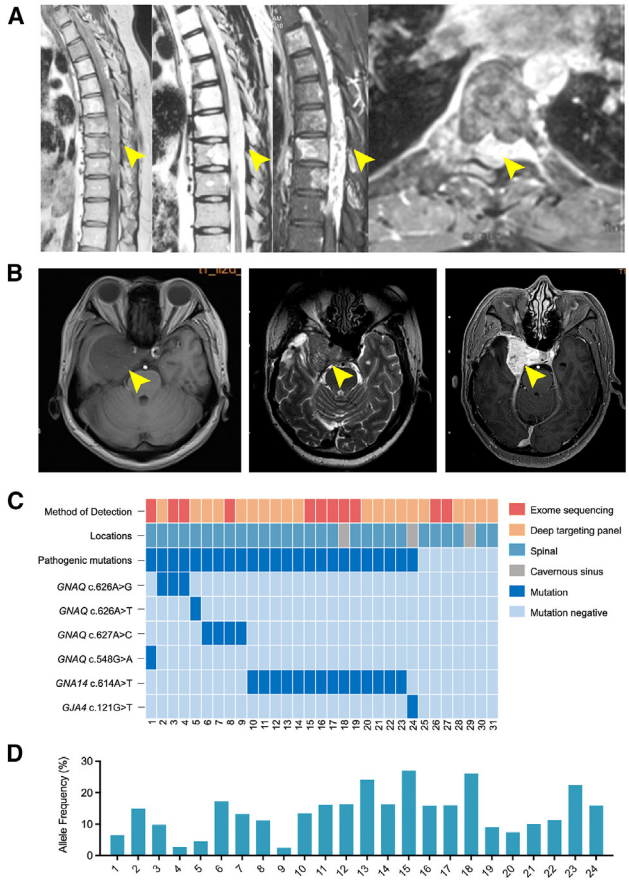

Figure 1. Detection of pathogenic mutations in samples obtained from individuals with extra-axial cavernous hemangiomas

(A) The MRI appearance of a case of spinal cavernous hemangiomas that involved the vertebra and epidural space in thoracic segments (yellow arrowhead). The lesions appear hypointense on T1-weighted images and hyperintense on T2-weighted images, with obvious enhancement following the administration of contrast medium.

(B) The MRI appearance of a case of cavernous sinus cavernous hemangiomas located at the right cavernous sinus (yellow arrowhead) with mass effect to the right temporal lobe.

(C) The detection of the pathogenic mutations on WES or deep targeting panel. Among the 31 tissue samples obtained from extra-axial cavernous hemangiomas in our study, somatic missense variants in *GNA14*, *GNAQ*, or *GJA4* in 24 samples were identified, accounting for 77.4% of cases.

(D) The allele frequency of the pathogenic mutations on WES or deep targeting panel.

Phenotype of ECs with *GNAQ* and *GNA14* mutations

To investigate the influence of GNAQ p.Gln209Arg and GNA14 p.Gln205Leu expression on ECs, we transfected HUVECs with lentiviruses expressing *GNAQ* c.626A>G, *GNAQ* WT, *GNA14* c.614A>T, *GNA14* WT ,or empty vector constructs. In the *in vitro* cell-tube formation assay, we observed that total length of the blood vessels formed by cells with GNAQ p.Gln209Arg was significantly increased compared to GNAQ WT (Figures 3A and 3B). However, ECs with GNA14 p.Gln205Leu did not induce significant increase of total length of the blood vessels compared to ECs with GNA14 WT (Figures 3C and 3D). Previous literature has indicated the enrichment of GNAQ p.Arg183Gln in ECs within capillary malformations found in skin and Sturge-Weber syndrome-affected brains.[34] To investigate whether endothelial expression of GNAQ p.Gln209Arg or GNA14 p.Gln205Leu alone is sufficient to induce the formation of enlarged blood vessels, we co-cultured ECs with GNAQ p.Gln209Arg, GNA14 p.Gln205Leu, GNAQ WT, or GNA14 WT cells with human retinal pigment epithelial cells within Matrigel and subsequently injected this cell/Matrigel mixture into the flanks of nude mice. After a 12-day period, the implanted constructs were excised, photographed, and sectioned for histological examination through H&E staining. Both ECs with GNAQ p.Gln209Arg and GNA14 p.Gln205Leu implants displayed a significantly higher degree of vascularization compared to ECs with GNAQ WT or ECs with GNA14 WT implants. H&E staining revealed the presence of numerous red blood cell-filled vessels, indicative of a connection with the mouse circulatory system (Figures 3E and 3F). The results showed that the expressions of GNAQ p.Gln209Arg and GNA14 p.Gln205Leu in ECs result in significant dilation of vascular lumen.

To identify the impact of signaling pathways on ECs with GNAQ p.Gln209Arg and GNA14 p.Gln205Leu, we performed RNA sequencing of HUVECs expressing GNAQ p.Gln209Arg and GNA14 p.Gln205Leu, or GNAQ WT and GNA14 WT (with $n = 3$ biological replicates per group) (Figures 4A–4D). Kyoto Encyclopedia of Genes and Genomes (KEGG) and Gene Ontology Biological Pathways (GO-BP) revealed an enrichment of genes involved in the categories of angiogenesis, blood vessel development, and MAPK pathways in the ECs with GNAQ p.Gln209Arg (Figure 4C), ECs with GNA14 p.Gln205Leu group compared to the ECs with GNAQ WT, or ECs with GNA14 WT (Figure 4D). Particularly, we observed significant upregulation of the PI3K-AKT-mTOR pathways in ECs expressing GNAQ p.Gln209Arg compared to the wild type, and significant upregulation of the MAPK and angiogenesis-related pathways in the transcriptomic data of ECs with GNA14 p.Gln205Leu (Figures 4C and 4D). The expression of angiogenesis-related genes was found to be up-regulated (Figure S4). Additionally, we conducted a comparative analysis of RNA-sequencing data between ECs with GNAQ p.Gln209Arg and those with GNA14 p.Gln205Leu (Figures 4E and 4F). Our findings revealed significant differences in the PI3K-AKT-mTOR pathway, MAPK pathway, TGF-beta pathway, and angiogenesis-related pathways in ECs expressing GNAQ p.Gln209Arg compared to those with GNA14 p.Gln205Leu (Figure 4G). Comparative data analysis was also performed by integrating self-test samples (GNAQ p.Gln209Arg and GNAQ WT) with RNA-sequencing data obtained from the GEO data repository (GEO: GSE199978), after mitigating batch effects. This analysis highlighted similar significant differences in the expression of the aforementioned pathways, including the PI3K-AKT signaling pathway, MAPK signaling pathway, TGF-beta signaling

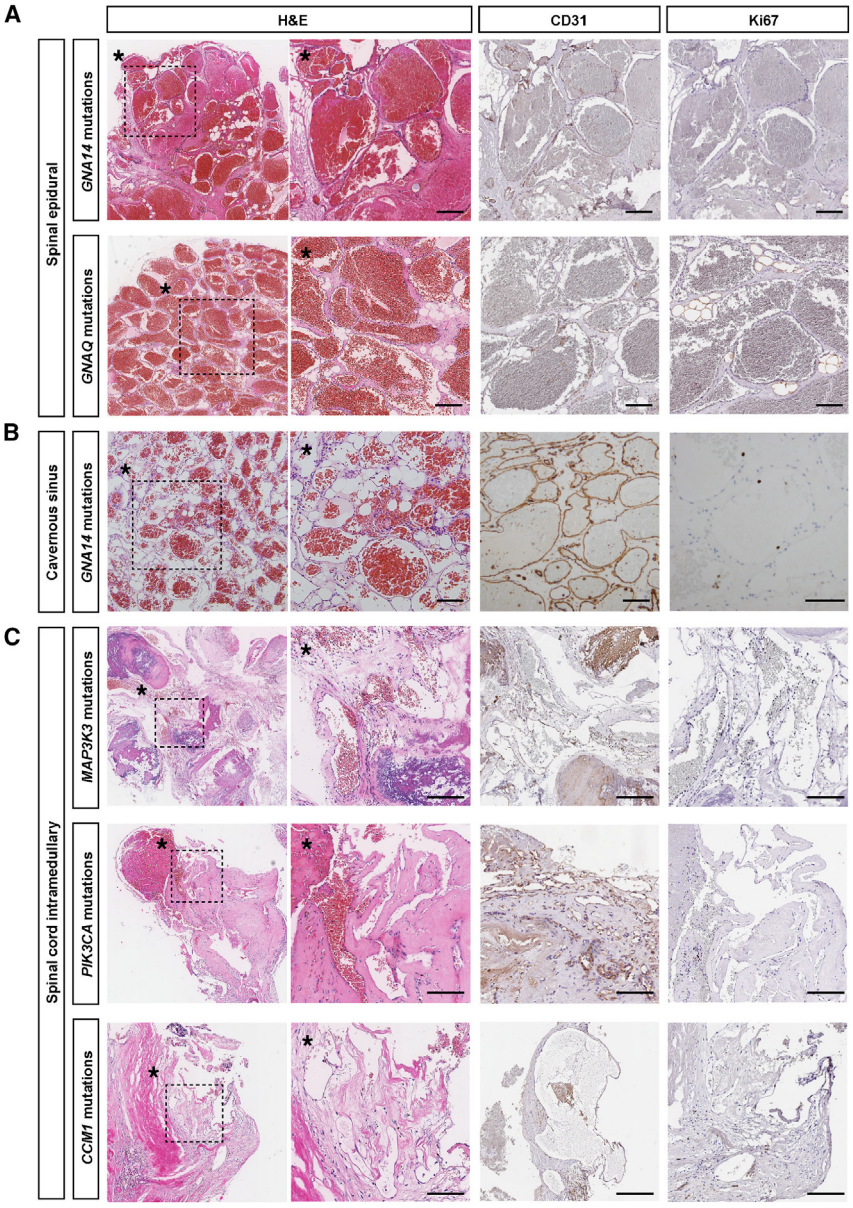

Figure 2. Pathological characterization of ECHs with *GNAQ* or *GNA14* mutations, in comparison with spinal cord intramedullary cavernous malformations with *MAP3K3*, *PIK3CA*, or *CCM1* mutations

(A) H&E staining and CD31 and Ki67 immunohistochemical staining on paraffin-embedded samples of spinal epidural cavernous hemangiomas with *GNAQ* or *GNA14* mutations. The lesions exhibited widely dilated thin-walled vessels lined by a single layer of CD31-positive endothelial cells, interspersed among adipocytes, indicative of cavernous hemangiomas. Ki67 staining revealed rare occurrences of positive $Ki67^{+}$ endothelial cells (scale bar, 100 μm).

(B) The H&E staining, CD31, and Ki67 immunohistochemical staining on paraffin-embedded samples of cavernous sinus cavernous hemangiomas with *GNA14* mutations. The lesions exhibited widely dilated thin-walled vessels lined by a single layer of CD31-positive endothelial cells, interspersed among adipocytes, indicative of cavernous hemangiomas. Ki67 staining revealed rare occurrences of $Ki67^{+}$ endothelial cells (scale bar, 100 μm).

(C) The H&E staining, CD31, and Ki67 immunohistochemical staining on paraffin-embedded samples of spinal cord intramedullary cavernous malformations with *MAP3K3*, *PIK3CA*, or *CCM1* mutations. Spinal cord intramedullary cavernous malformations exhibited widely dilated thin-walled vessels lined by a single layer of CD31-positive endothelial cells with obvious hemosiderin deposits (scale bar, 100 μm).

pathway, focal adhesion, fluid shear stress and atherosclerosis, and angiogenesis-related pathways (Figure S3). The potential role of *ANGPT2* overexpression had been identified in vascular malformations, and raises the possibility that it contributes to the enlargement of blood vessels observed in the extra-axial cavernous hemangiomas.[35–37] ANGPT2 abundance was notably elevated in GNAQ p.Gln209Arg ECs compared to GNAQ WT ECs(Figure S4).

Rapamycin treatment in one person with *GNAQ* mutant ECH

A14-year-old female experienced progressive weakness in both her lower extremities and numbness in the bilateral plantar region for two months before admission. She had no specific personal or family medical history. Upon physical examination, multiple port-wine stain skin nevi were observed on her bilateral extremities, chest, and midback (Figure 4). Neurological examination revealed grade 3/5 motor strength in the bilateral lower extremities, positive bilateral Babinski signs, and decreased superficial sensation in response to pain, temperature, and touch. Magnetic resonance imaging of the thoracic and lumbar spine revealed multiple enhancing epidural lesions between T4-T6 and T11-S3, causing severe compression of the spinal cord. Additionally, the vertebral bodies at the same metamere were also affected (Figure 5B). Due to the extensive lesion distribution and the associated high surgical risk, surgical resection of the lesions was deemed to be unsuitable for the person. Consequently, the person underwent biopsy procedures on both the epidural lesions and associated cutaneous lesions. Pathological examination revealed that both the epidural and cutaneous lesions featured blood-filled sinusoidal channels lined by a single layer of flattened ECs interspersed among adipocytes, indicating cavernous hemangiomas (Figure 5C). WES was conducted on fresh-frozen tissue samples from both the epidural and cutaneous lesions. The average sequencing depth reached 300×. Pathogenic mutations in the *GNAQ*

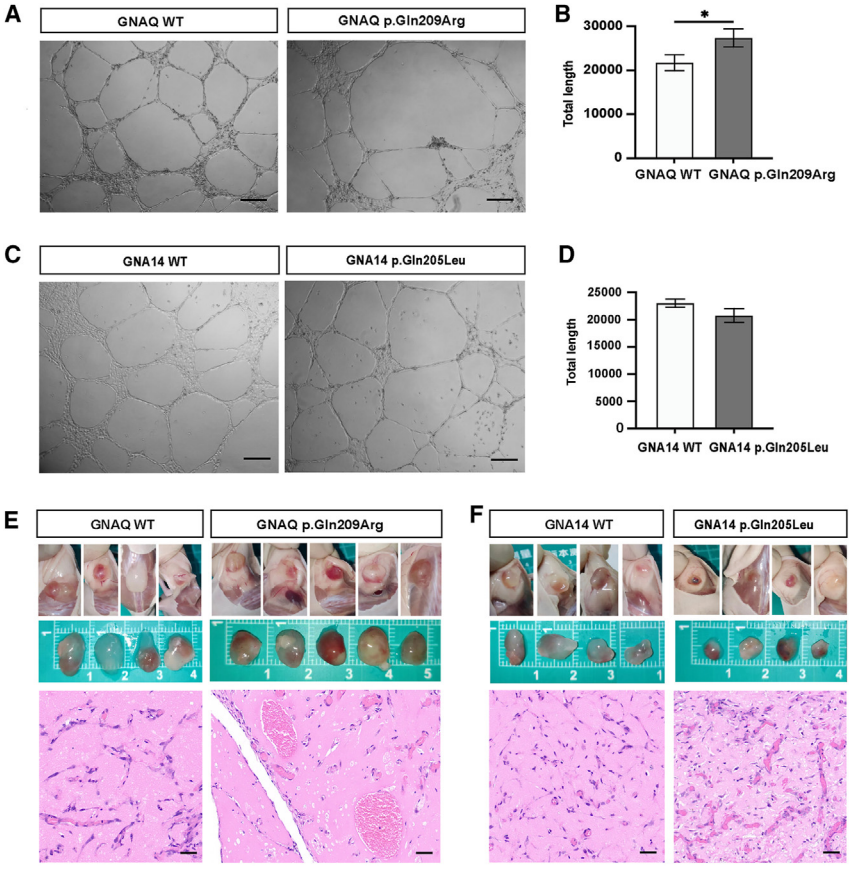

Figure 3. Phenotype of GNAQ p.Gln209Arg and GNA14 p.Gln205Leu ECs

(A) In the cell-tube formation assay, GNAQ p.Gln209Arg ECs showed an increase in the total length of the forming vessel compared to GNAQ WT ECs (scale bar, 100 μm).

(B) Quantification of cell-tube formation assay of GNAQ p.Gln209Arg ECs compared to GNAQ WT ECs. The biological replicates were three for each group, $n = 3$. $^*p < 0.05$, unpaired two-sided Student's t test. Data are represented as the mean ± SD.

(C) There were no significant changes between ECs with GNA14 p.Gln205Leu or GNA14 WT (scale bar, 100 μm).

(D) Quantification of cell-tube formation assay of the ECs with GNA14 p.Gln205Leu compared to ECs with GNA14 WT. The biological replicates were three for each group, $n = 3$. Data are represented as the mean ± SD.

(E) The enlarged blood vessel lesions assembled by ECs with GNAQ p.Gln209Arg and GNA14 p.Gln205Leu in xenograft models. H&E staining showed enlarged blood vessels throughout the implants and appearance of enlarged vessels in GNAQ p.Gln209Arg implants compared with GNAQ WT implants (scale bar, 50 μm).

(F) Implants with GNA14 p.Gln205Leu showed significantly more blood vessels compared with implants with GNA14 WT (scale bar, 50 μm).

(GenBank: NM_002072.5; c.626A>G [p.Gln209Arg]) were identified in both the epidural and cutaneous lesions, with an allele frequency of 2.7% in epidural cavernous hemangiomas and 4.3% in cutaneous cavernous hemangiomas.

Rapamycin, an mTOR inhibitor approved by the US Food and Drug Administration, has shown promise as a targeted pharmacological treatment for vascular malformations, including low-flow venous malformations and *GNAQ* mutant Sturge-Weber syndrome.[10,38,39] Based on our *in vitro* findings showing a notable upregulation of the PI3K-AKT-mTOR and angiogenesis-related pathways in ECs expressing GNAQ p.Gln209Arg (Figure 4C), the person received a prescription for an oral rapamycin regimen at 1.5 mg per day, subsequent to obtaining written consent. Dose adjustments were determined by monthly monitoring of serum rapamycin levels, aiming to achieve a targeted range of 4–12 ng/mL. Over the course of one year of treatment, a gradual regression of cutaneous cavernous hemangiomas in terms of both volume and color was observed (Figure 5D). Furthermore, the motor strength of the bilateral lower extremities improved from grade 3 to grade 4. We utilized the SF-36 health survey to evaluate the person's recovery. After 340 days of treatment with rapamycin, the person exhibited a noteworthy enhancement in physical functioning, role-physical, general health, social functioning, and health transition (Table S3). Serial spinal MRIs during follow-up showed no significant changes in the vertebral and epidural lesions (Figure 5E). Throughout the treatment period, the person experienced occasional oral ulcers as the primary side effect, with no other significant adverse effects noted. These results suggest that targeted therapy may represent a viable therapeutic approach for individuals with complex *GNAQ* mutant cavernous hemangiomas.

Discussion

GNAQ and *GNA14* belong to the same gene family of G protein α-subunit genes. They encode the α-subunit of heterotrimeric G proteins (Gαq).[40] These proteins play a crucial role in intracellular signaling pathways, particularly those involving G protein-coupled receptors (GPCRs).[41] Our data show that spinal and intracranial extra-axial cavernous hemangiomas mainly result from activating mutations in *GNAQ* and *GNA14*. Mutations in *GNAQ* and *GNA14* dysregulate angiogenesis and cause enlarged blood vessels in the extra-axial cavernous hemangiomas. The regression of the lesions in the person with complex *GNAQ* mutant spinal epidural cavernous hemangiomas after the treatment of rapamycin showed that targeted therapy may represent a viable therapeutic approach, especially for individuals with complex and inoperable cavernous hemangiomas.

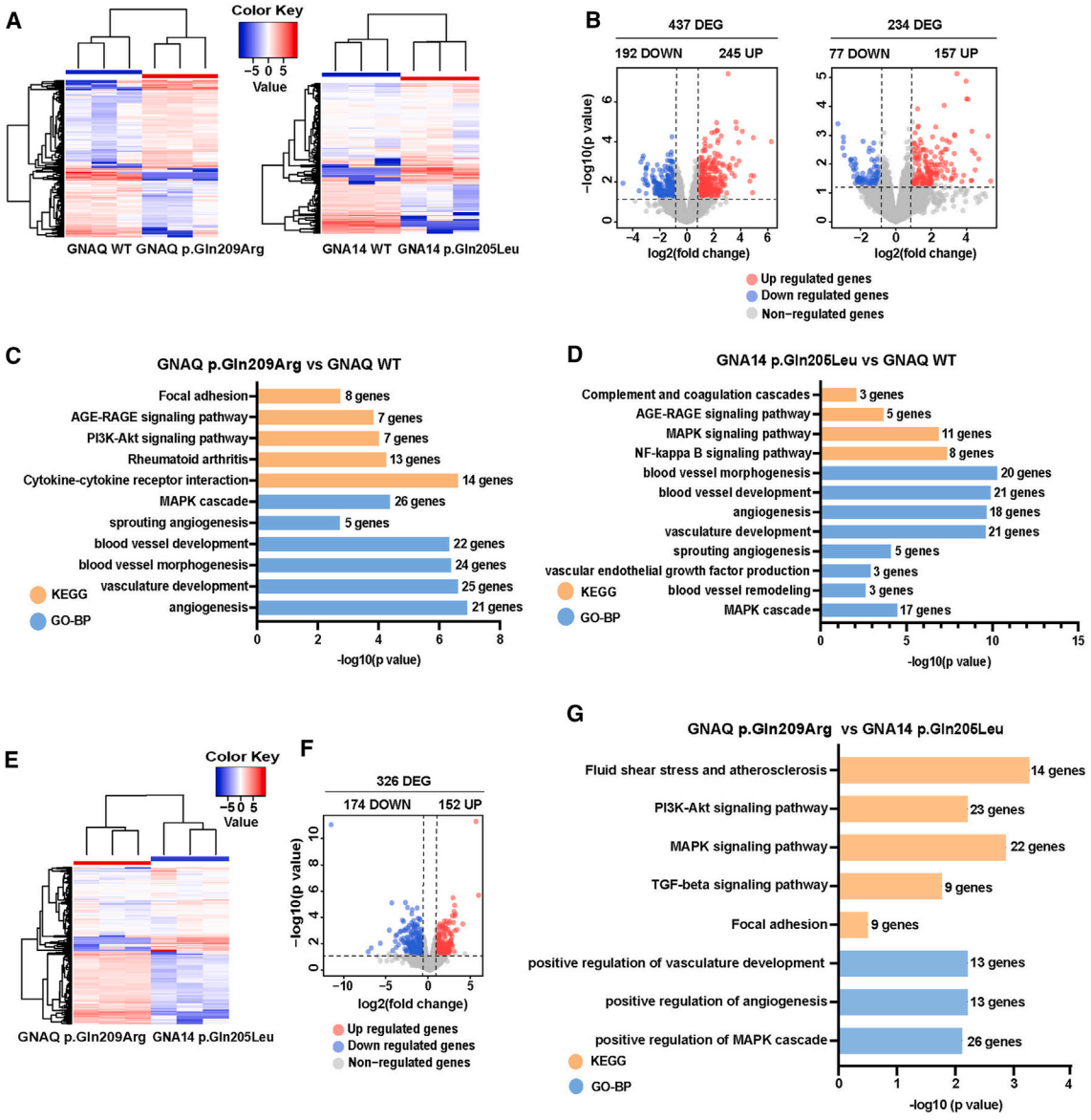

Figure 4. Bulk RNA-sequencing GNAQ p.Gln209Arg and GNA14 p.Gln205Leu ECs

(A) The heat maps display differentially expressed transcripts as measured by bulk RNA sequencing in ECs with GNAQ p.Gln209Arg (left) and GNA14 p.Gln205Leu (right) compared to ECs with GNAQ WT and GNA14 WT. DEGs are defined as having a log2 (fold change) ≥ 1 and an adjusted p value of <0.05. Each group consisted of three biological replicates.

(B) Volcano plots illustrate downregulated (blue) and upregulated (red) genes in ECs with GNAQ p.Gln209Arg compared to ECs with GNAQ WT (left) and in ECs with GNA14 p.Gln205Leu compared to ECs with GNA14 WT (right).

(C) KEGG and GO-BP enrichment analyses of DEGs in ECs with GNAQ p.Gln209Arg compared to ECs with GNAQ WT. KEGG analysis reveals increased expression of relevant genes in the PI3K-AKT-mTOR pathway in ECs with GNAQ p.Gln209Arg compared to ECs with GNAQ WT. GO-BP analysis shows increased expression of relevant genes in the MAPK and angiogenesis-related pathways in GNAQ p.Gln209Arg Ecs compared to GNAQ WT ECs.

(D) KEGG and GO-BP pathway analyses of DEGs in GNA14 p.Gln205Leu ECs compared to GNA14 WT ECs. KEGG analysis demonstrates increased expression of relevant genes in the MAPK pathway and NF-κB pathway in GNA14 p.Gln205Leu ECs compared to GNA14 WT ECs. GO-BP analysis indicates increased expression of relevant genes in the MAPK and angiogenesis-related pathways in GNA14 p.Gln205Leu ECs compared to GNA14 WT ECs.

(E) The heat maps display differentially expressed transcripts as measured by bulk RNA sequencing in GNAQ p.Gln209Arg ECs (left) compared to GNA14 p.Gln205Leu ECs (right).

(F) Volcano plot illustrates downregulated (blue) and upregulated (red) genes in GNAQ p.Gln209Arg ECs compared to GNA14 p.Gln205Leu ECs.

(G) KEGG and GO-BP enrichment analyses of DEGs in GNAQ p.Gln209Arg ECs compared to GNA14 p.Gln205Leu ECs. KEGG analysis reveals differential expression of relevant genes in the PI3K-AKT-mTOR pathway and MAPK pathway. GO-BP analysis shows differential expression of relevant genes in angiogenesis-related pathways.

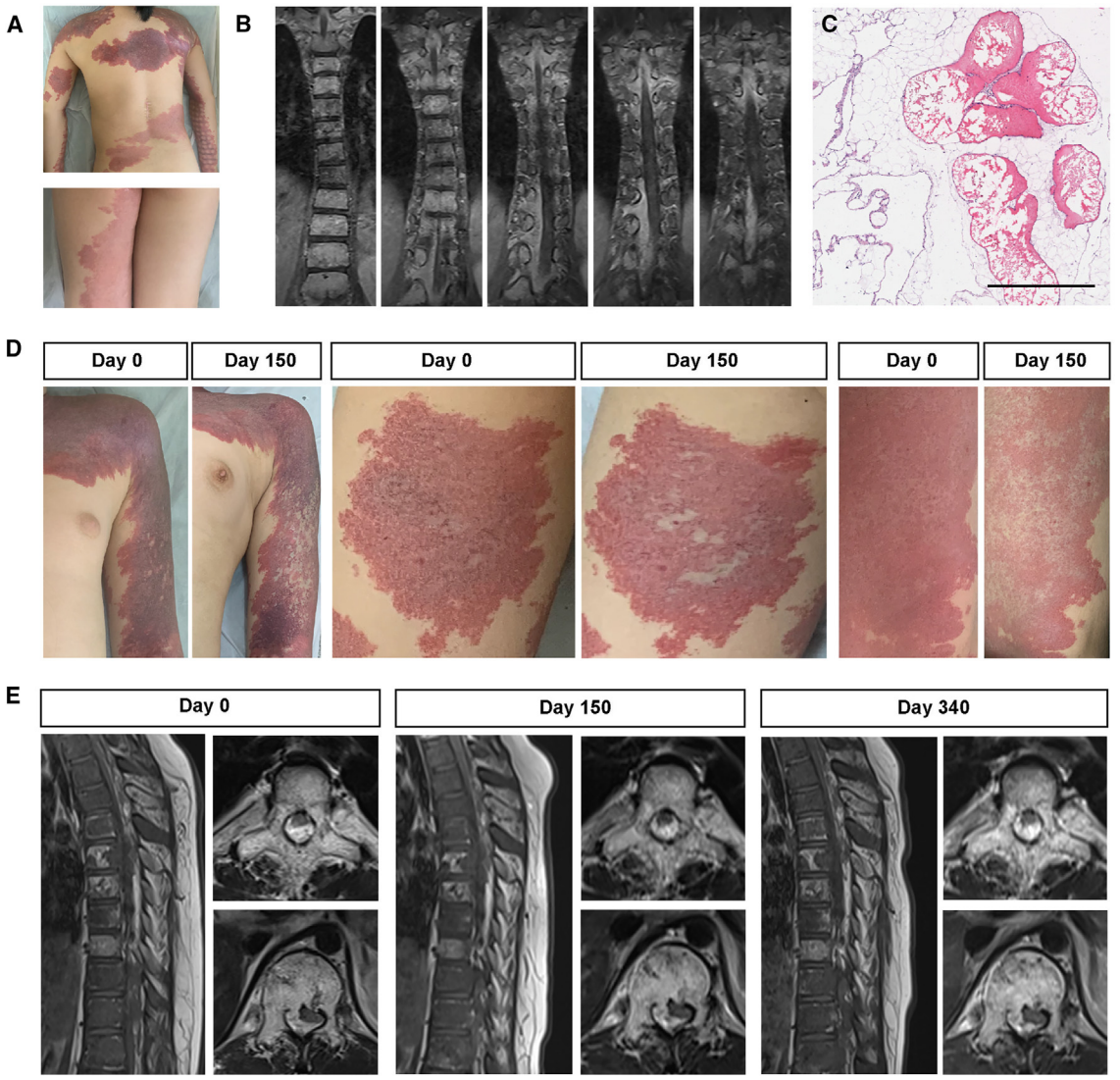

Figure 5. Rapamycin treatment in one individual with *GNAQ* mutant spinal epidural cavernous hemangiomas
(A) Multiple port-wine stain skin nevi on the proband's bilateral extremities, chest, and midback.
(B) The MRI of the thoracic and lumbar spine revealed multiple enhancing epidural lesions between T4-T6 and T11-S3 in a 14-year-old female.
(C) The epidural lesions featured blood-filled sinusoidal channels lined by a single layer of flattened endothelial cells interspersed among adipocytes, indicative of cavernous hemangiomas (scale bar, 500 μm).
(D) A gradual regression of cutaneous cavernous hemangiomas in terms of both volume and color during the treatment of rapamycin.
(E) Serial spinal MRIs during follow-up identifying no significant changes in the vertebral and epidural lesions.

Prior research has established that mutations in *GNA14*, *GNA11*, and *GNAQ* are mutually exclusive.[42] Among the *GNAQ* homologs, *GNA11* and *GNA14* exhibit the highest amino acid sequence similarity to *GNAQ*.[43] Activating mutations in G protein α-subunit genes has been implicated in melanocytic tumors and vascular lesions.[34,43–48] Notably, within melanocytic tumors, a majority of uveal melanomas and blue nevi harbor activating mutations at codon 183 or 209 of *GNAQ*.[46] While *GNA14* mutations have not been detected in melanocytic tumors, *GNA14* c.614A>T mutations have been identified in various vascular tumors.[42,43] Our data show that extra-axial cavernous hemangiomas, including spinal epidural cavernous hemangiomas and cavernous sinus cavernous hemangiomas also result from activating mutations in G protein α-subunit genes.

Gαq connects seven-transmembrane domain receptors on the cell membrane to intracellular signaling pathways.[46] Gαq activation is known to be associated with various signaling pathways, including PI3K-AKT-mTOR and MAPK pathways, promoting functions such as cell proliferation and protein synthesis.[49] Our transcriptomic data showed pronounced upregulation of the PI3K-AKT-mTOR Ras and angiogenesis-related pathways in ECs expressing GNAQ p.Gln209Arg compared to the wild type. Among individuals with *GNAQ* mutant cavernous hemangiomas at our center, a 14-year-old female undergoing one year of rapamycin treatment, targeting PI3K-AKT-mTOR

pathways, experienced gradual regression in size and color of *GNAQ* mutant cutaneous cavernous hemangiomas. These results suggest that targeted therapy may be a viable therapeutic option for individuals with complex *GNAQ* mutant cavernous hemangiomas.

We found *GJA4* c.121G>T somatic mutations in one case of cavernous sinus hemangiomas, yet no instances of *GJA4* c.121G>T somatic mutations were detected in spinal epidural cavernous hemangiomas. *GJA4* c.121G>T mutations have been observed in orbital cavernous venous malformations and intracranial extra-axial cavernous hemangiomas in prior studies.[11,12] *GJA4* encodes connexin 37, a protein integral to gap junctions that forms intercellular channels between ECs and regulates cell cycle in the vasculature.[50–53] Prior studies demonstrated that the *GJA4* c.121G>T mutations correlated with dysregulation of the Cx37-SGK1 pathway, leading to endothelial cell hyperproliferation, abnormal venous angiogenesis, and dilated venous lumens.[11,12] While direct interactions between Cx37-SGK1 signaling and GNA proteins lack extensive documentation, unraveling the mechanisms behind the comparable phenotype observed in *GNAQ*, *GNA14*, and *GJA4* mutant cavernous hemangiomas demands further investigation.

The classification of ECHs as either vascular tumors or vascular malformations, akin to cavernous malformations, has sparked debate within the medical community.[54] Cavernous malformations are well-defined venous malformations found within the central nervous system (CNS) and are generally considered non-neoplastic.[55] Conversely, extra-axial cavernous hemangiomas exhibit progressive growth over time, resulting in distortion and compression of surrounding tissues—a behavior more characteristic of neoplastic lesions. Unlike intra-axial cavernous malformations, extra-axial cavernous hemangiomas typically do not present with acute bleeding but rather become symptomatic due to lesion compression.[56] Histologically, both cavernous malformations and extra-axial hemangiomas feature dilated channels lined with a single layer of endothelium and lack smooth muscle or elastic fibers. However, extra-axial hemangiomas may be larger and contain vascular channels devoid of thrombosis, calcification, and hemosiderin-laden macrophages, indicative of a high-flow state.[54] Therapeutically, there was also a difference in sensitivity to radiotherapy between extra-axial hemangiomas and intra-axial cavernous malformations.[57,58] Furthermore, genetic studies have revealed distinct mutations in extra-axial cavernous hemangiomas (such as *GNAQ*, *GNA14*, and *GJA4*) compared to those in intra-axial cavernous malformations (such as *CCM1-3*, *MAP3K3*, and *PIK3CA*), further highlighting their differences.[6–10] To mitigate confusion and enhance clarity, physicians commonly refer to lesions occurring within the CNS as "cavernous malformations" and those in extra-axial locations as "cavernous hemangiomas."[54,56,59] This terminology helps delineate the distinct nature of these two entities and aids in their understanding among medical professionals. Given the efficiency of radiotherapy in treating cavernous sinus cavernous hemangiomas and the identification of similar somatic mutations and pathological characteristics in both spinal epidural cavernous hemangiomas and cavernous sinus cavernous hemangiomas in our study, we suggest that radiotherapy might also be effective for spinal epidural cavernous hemangiomas.

In our cohort, we also observed individuals with cutaneous cavernous hemangiomas harboring the same *GNAQ* somatic mutations as those found in spinal epidural cavernous hemangiomas. This metameric phenotype resembles previously reported conditions such as Cobb syndrome (spinal arteriovenous metameric syndrome) and cerebrofacial vascular metameric syndrome.[60–64] However, the mechanisms underlying metameric vascular syndromes remain unclear. We hypothesize that the common somatic mutations observed in both spinal epidural cavernous hemangiomas and cutaneous cavernous hemangiomas may originate from precursor cells with *GNAQ* mutations during embryonic development and migrate along the mesoderm during vasculogenesis.[65]

Our research sheds light on the biological mechanisms underlying extra-axial cavernous hemangiomas. Rather than germline mutations in the *CCM1*, *CCM2*, *CCM3*, and somatic mutations in *MAP3K3* and *PIK3CA* playing a major causative role in cerebral and spinal cord cavernous malformations, somatic mutations in *GNA* predominated in ECHs. This result, which was supported by findings in a preclinical model, and off label use of rapamycin in an individual with *GNAQ* mutant cavernous hemangiomas offers potential for the development of targeted therapies for the treatment of complex extra-axial cavernous hemangiomas that are refractory to surgery and radiotherapy.

Data and code availability

The datasets supporting the current study have not been deposited in a public repository because of institutional ethics restrictions but are available from the corresponding author on request.

Supplemental information

Supplemental information can be found online at https://doi.org/10.1016/j.ajhg.2024.05.020.

Acknowledgments

This work was supported by the National Natural Science Foundation of China with grants 82220108010 and 81971113 to Hongqi Zhang, grants 82330038, 82122020, and 81971104 to T.H., grant 82201440 to J.R., and grant 82201439 to J.Y., grant 81701796 to Y.L.; Beijing Municipal Science and Technology Commission with grant D161100003816001 to Hongqi Zhang and grant Z201100005520024 to T.H.; Beijing Municipal Education Commission with grant BPHR20220113 to Hongqi Zhang; Capital's

Funds for Health Improvement and Research with grant 2022-2Z-20110 to Hongqi Zhang; and Beijing Hospitals Authority Youth Program with grant QML20230804 to Y.L. We thank all the individuals and their families for participating in our study and for offering all information and data.

Author contributions

T.H., J.R., and Hongqi Zhang conceived the project. J.R., T.H., Hongqi Zhang, D.X., and M.L.K. designed experiments. Z.C. and Y.R. performed all *in vitro* and *in vivo* experiments. J.R., L.W., Y.G., C.J., Y.R., S.Z., T.T., J.Y., Y.L., W.D., J.G., and K.W. performed the other experiments and data analysis. W.D., J.G., K.W., and Hongdian Zhang provided cases. J.R., Z.C., and C.J. wrote the manuscript. All authors reviewed and edited the manuscript.

Declaration of interests

The authors declare no competing interests.

Received: February 15, 2024
Accepted: May 22, 2024
Published: June 24, 2024

Web resources

GenBank, https://www.ncbi.nlm.nih.gov/genbank/
GEO, http://www.ncbi.nlm.nih.gov/geo/
OMIM, https://www.omim.org/

References

1. Biondi, A., Clemenceau, S., Dormont, D., Deladoeuille, M., Ricciardi, G.K., Mokhtari, K., Sichez, J.P., and Marsault, C. (2002). Intracranial extra-axial cavernous (HEM) angiomas: tumors or vascular malformations? J. Neuroradiol. *29*, 91–104.
2. Gao, C., Xu, W., Qing Lian, J., Feng, D., Cui, J.F., and Liu, H. (2018). Spinal Epidural Cavernous Hemangioma: A Clinical Series of 7 Patients. World Neurosurg. *111*, e183–e191. https://doi.org/10.1016/j.wneu.2017.12.006.
3. Vasudeva, V.S., Chi, J.H., and Groff, M.W. (2016). Surgical treatment of aggressive vertebral hemangiomas. Neurosurg. Focus *41*, E7. https://doi.org/10.3171/2016.5.FOCUS16169.
4. Meyer, F.B., Lombardi, D., Scheithauer, B., and Nichols, D.A. (1990). Extra-axial cavernous hemangiomas involving the dural sinuses. J. Neurosurg. *73*, 187–192. https://doi.org/10.3171/jns.1990.73.2.0187.
5. Akers, A., Al-Shahi Salman, R., A Awad, I., Dahlem, K., Flemming, K., Hart, B., Kim, H., Jusue-Torres, I., Kondziolka, D., Lee, C., et al. (2017). Synopsis of Guidelines for the Clinical Management of Cerebral Cavernous Malformations: Consensus Recommendations Based on Systematic Literature Review by the Angioma Alliance Scientific Advisory Board Clinical Experts Panel. Neurosurgery *80*, 665–680. https://doi.org/10.1093/neuros/nyx091.
6. Peyre, M., Miyagishima, D., Bielle, F., Chapon, F., Sierant, M., Venot, Q., Lerond, J., Marijon, P., Abi-Jaoude, S., Le Van, T., et al. (2021). Somatic PIK3CA Mutations in Sporadic Cerebral Cavernous Malformations. N. Engl. J. Med. *385*, 996–1004. https://doi.org/10.1056/NEJMoa2100440.
7. Snellings, D.A., Hong, C.C., Ren, A.A., Lopez-Ramirez, M.A., Girard, R., Srinath, A., Marchuk, D.A., Ginsberg, M.H., Awad, I.A., and Kahn, M.L. (2021). Cerebral Cavernous Malformation: From Mechanism to Therapy. Circ. Res. *129*, 195–215. https://doi.org/10.1161/CIRCRESAHA.121.318174.
8. Hong, T., Xiao, X., Ren, J., Cui, B., Zong, Y., Zou, J., Kou, Z., Jiang, N., Meng, G., Zeng, G., et al. (2021). Somatic MAP3K3 and PIK3CA mutations in sporadic cerebral and spinal cord cavernous malformations. Brain *144*, 2648–2658. https://doi.org/10.1093/brain/awab117.
9. Weng, J., Yang, Y., Song, D., Huo, R., Li, H., Chen, Y., Nam, Y., Zhou, Q., Jiao, Y., Fu, W., et al. (2021). Somatic MAP3K3 mutation defines a subclass of cerebral cavernous malformation. Am. J. Hum. Genet. *108*, 942–950. https://doi.org/10.1016/j.ajhg.2021.04.005.
10. Ren, A.A., Snellings, D.A., Su, Y.S., Hong, C.C., Castro, M., Tang, A.T., Detter, M.R., Hobson, N., Girard, R., Romanos, S., et al. (2021). PIK3CA and CCM mutations fuel cavernomas through a cancer-like mechanism. Nature *594*, 271–276. https://doi.org/10.1038/s41586-021-03562-8.
11. Huo, R., Yang, Y., Xu, H., Zhao, S., Song, D., Weng, J., Ma, R., Sun, Y., Wang, J., Jiao, Y., et al. (2023). Somatic GJA4 mutation in intracranial extra-axial cavernous hemangiomas. Stroke Vasc. Neurol. *8*, 453–462. https://doi.org/10.1136/svn-2022-002227.
12. Hongo, H., Miyawaki, S., Teranishi, Y., Mitsui, J., Katoh, H., Komura, D., Tsubota, K., Matsukawa, T., Watanabe, M., Kurita, M., et al. (2023). Somatic GJA4 gain-of-function mutation in orbital cavernous venous malformations. Angiogenesis *26*, 37–52. https://doi.org/10.1007/s10456-022-09846-5.
13. Sebold, A.J., Day, A.M., Ewen, J., Adamek, J., Byars, A., Cohen, B., Kossoff, E.H., Mizuno, T., Ryan, M., Sievers, J., et al. (2021). Sirolimus Treatment in Sturge-Weber Syndrome. Pediatr. Neurol. *115*, 29–40. https://doi.org/10.1016/j.pediatrneurol.2020.10.013.
14. Bolger, A.M., Lohse, M., and Usadel, B. (2014). Trimmomatic: a flexible trimmer for Illumina sequence data. Bioinformatics *30*, 2114–2120. https://doi.org/10.1093/bioinformatics/btu170.
15. Li, H., and Durbin, R. (2009). Fast and accurate short read alignment with Burrows-Wheeler transform. Bioinformatics *25*, 1754–1760. https://doi.org/10.1093/bioinformatics/btp324.
16. Li, H., Handsaker, B., Wysoker, A., Fennell, T., Ruan, J., Homer, N., Marth, G., Abecasis, G., Durbin, R.; and 1000 Genome Project Data Processing Subgroup (2009). The Sequence Alignment/Map format and SAMtools. Bioinformatics *25*, 2078–2079. https://doi.org/10.1093/bioinformatics/btp352.
17. McKenna, A., Hanna, M., Banks, E., Sivachenko, A., Cibulskis, K., Kernytsky, A., Garimella, K., Altshuler, D., Gabriel, S., Daly, M., and DePristo, M.A. (2010). The Genome Analysis Toolkit: a MapReduce framework for analyzing next-generation DNA sequencing data. Genome Res. *20*, 1297–1303. https://doi.org/10.1101/gr.107524.110.
18. Cibulskis, K., Lawrence, M.S., Carter, S.L., Sivachenko, A., Jaffe, D., Sougnez, C., Gabriel, S., Meyerson, M., Lander, E.S., and Getz, G. (2013). Sensitive detection of somatic point mutations in impure and heterogeneous cancer samples. Nat. Biotechnol. *31*, 213–219. https://doi.org/10.1038/nbt.2514.
19. 1000 Genomes Project Consortium, Auton, A., Brooks, L.D., Durbin, R.M., Garrison, E.P., Kang, H.M., Korbel, J.O., Marchini, J.L., McCarthy, S., McVean, G.A., and Abecasis, G.R. (2015). A global reference for human genetic variation. Nature *526*, 68–74. https://doi.org/10.1038/nature15393.

20. Sherry, S.T., Ward, M.H., Kholodov, M., Baker, J., Phan, L., Smigielski, E.M., and Sirotkin, K. (2001). dbSNP: the NCBI database of genetic variation. Nucleic Acids Res. *29*, 308–311. https://doi.org/10.1093/nar/29.1.308.
21. Fang, H., Bergmann, E.A., Arora, K., Vacic, V., Zody, M.C., Iossifov, I., O'Rawe, J.A., Wu, Y., Jimenez Barron, L.T., Rosenbaum, J., et al. (2016). Indel variant analysis of short-read sequencing data with Scalpel. Nat. Protoc. *11*, 2529–2548. https://doi.org/10.1038/nprot.2016.150.
22. Wang, K., Li, M., and Hakonarson, H. (2010). ANNOVAR: functional annotation of genetic variants from high-throughput sequencing data. Nucleic Acids Res. *38*, e164. https://doi.org/10.1093/nar/gkq603.
23. Ewels, P., Magnusson, M., Lundin, S., and Käller, M. (2016). MultiQC: summarize analysis results for multiple tools and samples in a single report. Bioinformatics *32*, 3047–3048. https://doi.org/10.1093/bioinformatics/btw354.
24. Koboldt, D.C., Chen, K., Wylie, T., Larson, D.E., McLellan, M.D., Mardis, E.R., Weinstock, G.M., Wilson, R.K., and Ding, L. (2009). VarScan: variant detection in massively parallel sequencing of individual and pooled samples. Bioinformatics *25*, 2283–2285. https://doi.org/10.1093/bioinformatics/btp373.
25. Gudmundsson, S., Singer-Berk, M., Watts, N.A., Phu, W., Goodrich, J.K., Solomonson, M., Genome Aggregation Database Consortium, Rehm, H.L., MacArthur, D.G., and O'Donnell-Luria, A. (2022). Variant interpretation using population databases: Lessons from gnomAD. Hum. Mutat. *43*, 1012–1030. https://doi.org/10.1002/humu.24309.
26. Patel, R.K., and Jain, M. (2012). NGS QC Toolkit: a toolkit for quality control of next generation sequencing data. PLoS One *7*, e30619. https://doi.org/10.1371/journal.pone.0030619.
27. Kim, D., Paggi, J.M., Park, C., Bennett, C., and Salzberg, S.L. (2019). Graph-based genome alignment and genotyping with HISAT2 and HISAT-genotype. Nat. Biotechnol. *37*, 907–915. https://doi.org/10.1038/s41587-019-0201-4.
28. Pertea, M., Pertea, G.M., Antonescu, C.M., Chang, T.C., Mendell, J.T., and Salzberg, S.L. (2015). StringTie enables improved reconstruction of a transcriptome from RNA-seq reads. Nat. Biotechnol. *33*, 290–295. https://doi.org/10.1038/nbt.3122.
29. Anders, S., and Huber, W. (2010). Differential expression analysis for sequence count data. Genome Biol. *11*, R106. https://doi.org/10.1186/gb-2010-11-10-r106.
30. Galeffi, F., Snellings, D.A., Wetzel-Strong, S.E., Kastelic, N., Bullock, J., Gallione, C.J., North, P.E., and Marchuk, D.A. (2022). A novel somatic mutation in GNAQ in a capillary malformation provides insight into molecular pathogenesis. Angiogenesis *25*, 493–502. https://doi.org/10.1007/s10456-022-09841-w.
31. Johnson, W.E., Li, C., and Rabinovic, A. (2007). Adjusting batch effects in microarray expression data using empirical Bayes methods. Biostatistics *8*, 118–127. https://doi.org/10.1093/biostatistics/kxj037.
32. Ritchie, M.E., Phipson, B., Wu, D., Hu, Y., Law, C.W., Shi, W., and Smyth, G.K. (2015). limma powers differential expression analyses for RNA-sequencing and microarray studies. Nucleic Acids Res. *43*, e47. https://doi.org/10.1093/nar/gkv007.
33. Schindelin, J., Arganda-Carreras, I., Frise, E., Kaynig, V., Longair, M., Pietzsch, T., Preibisch, S., Rueden, C., Saalfeld, S., Schmid, B., et al. (2012). Fiji: an open-source platform for biological-image analysis. Nat. Methods *9*, 676–682. https://doi.org/10.1038/nmeth.2019.
34. Shirley, M.D., Tang, H., Gallione, C.J., Baugher, J.D., Frelin, L.P., Cohen, B., North, P.E., Marchuk, D.A., Comi, A.M., and Pevsner, J. (2013). Sturge-Weber syndrome and port-wine stains caused by somatic mutation in GNAQ. N. Engl. J. Med. *368*, 1971–1979. https://doi.org/10.1056/NEJMoa1213507.
35. Crist, A.M., Zhou, X., Garai, J., Lee, A.R., Thoele, J., Ullmer, C., Klein, C., Zabaleta, J., and Meadows, S.M. (2019). Angiopoietin-2 Inhibition Rescues Arteriovenous Malformation in a Smad4 Hereditary Hemorrhagic Telangiectasia Mouse Model. Circulation *139*, 2049–2063. https://doi.org/10.1161/CIRCULATIONAHA.118.036952.
36. Jenny Zhou, H., Qin, L., Zhang, H., Tang, W., Ji, W., He, Y., Liang, X., Wang, Z., Yuan, Q., Vortmeyer, A., et al. (2016). Endothelial exocytosis of angiopoietin-2 resulting from CCM3 deficiency contributes to cerebral cavernous malformation. Nat. Med. *22*, 1033–1042. https://doi.org/10.1038/nm.4169.
37. Huang, L., Bichsel, C., Norris, A.L., Thorpe, J., Pevsner, J., Alexandrescu, S., Pinto, A., Zurakowski, D., Kleiman, R.J., Sahin, M., et al. (2022). Endothelial GNAQ p.R183Q Increases ANGPT2 (Angiopoietin-2) and Drives Formation of Enlarged Blood Vessels. Arterioscler. Thromb. Vasc. Biol. *42*, e27–e43. https://doi.org/10.1161/ATVBAHA.121.316651.
38. Castillo, S.D., Tzouanacou, E., Zaw-Thin, M., Berenjeno, I.M., Parker, V.E.R., Chivite, I., Milà-Guasch, M., Pearce, W., Solomon, I., Angulo-Urarte, A., et al. (2016). Somatic activating mutations in Pik3ca cause sporadic venous malformations in mice and humans. Sci. Transl. Med. *8*, 332ra43. https://doi.org/10.1126/scitranslmed.aad9982.
39. Boscolo, E., Limaye, N., Huang, L., Kang, K.T., Soblet, J., Uebelhoer, M., Mendola, A., Natynki, M., Seront, E., Dupont, S., et al. (2015). Rapamycin improves TIE2-mutated venous malformation in murine model and human subjects. J. Clin. Invest. *125*, 3491–3504. https://doi.org/10.1172/JCI76004.
40. Chen, H., Yao, W., Jin, D., Xia, T., Chen, X., Lei, T., Zhou, L., and Yang, Z. (2008). Cloning, expression pattern, chromosomal localization, and evolution analysis of Porcine gnaq, gna11, and gna14. Biochem. Genet. *46*, 398–405. https://doi.org/10.1007/s10528-008-9158-6.
41. Boesgaard, M.W., Harpsøe, K., Malmberg, M., Underwood, C.R., Inoue, A., Mathiesen, J.M., König, G.M., Kostenis, E., Gloriam, D.E., and Bräuner-Osborne, H. (2020). Delineation of molecular determinants for FR900359 inhibition of $G_{q/11}$ unlocks inhibition of $G\alpha_s$. J. Biol. Chem. *295*, 13850–13861. https://doi.org/10.1074/jbc.RA120.013002.
42. Liau, J.Y., Lee, J.C., Tsai, J.H., Chen, C.C., Chung, Y.C., and Wang, Y.H. (2019). High frequency of GNA14, GNAQ, and GNA11 mutations in cherry hemangioma: a histopathological and molecular study of 85 cases indicating GNA14 as the most commonly mutated gene in vascular neoplasms. Mod. Pathol. *32*, 1657–1665. https://doi.org/10.1038/s41379-019-0284-y.
43. Jansen, P., Müller, H., Lodde, G.C., Zaremba, A., Möller, I., Sucker, A., Paschen, A., Esser, S., Schaller, J., Gunzer, M., et al. (2021). GNA14, GNA11, and GNAQ Mutations Are Frequent in Benign but Not Malignant Cutaneous Vascular Tumors. Front. Genet. *12*, 663272. https://doi.org/10.3389/fgene.2021.663272.
44. Liau, J.Y., Tsai, J.H., Lan, J., Chen, C.C., Wang, Y.H., Lee, J.C., and Huang, H.Y. (2020). GNA11 joins GNAQ and GNA14 as a recurrently mutated gene in anastomosing hemangioma.

Virchows Arch. *476*, 475–481. https://doi.org/10.1007/s00428-019-02673-y.

45. Joseph, N.M., Brunt, E.M., Marginean, C., Nalbantoglu, I., Snover, D.C., Thung, S.N., Yeh, M.M., Umetsu, S.E., Ferrell, L.D., and Gill, R.M. (2018). Frequent GNAQ and GNA14 Mutations in Hepatic Small Vessel Neoplasm. Am. J. Surg. Pathol. *42*, 1201–1207. https://doi.org/10.1097/PAS.0000000000001110.
46. Van Raamsdonk, C.D., Griewank, K.G., Crosby, M.B., Garrido, M.C., Vemula, S., Wiesner, T., Obenauf, A.C., Wackernagel, W., Green, G., Bouvier, N., et al. (2010). Mutations in GNA11 in uveal melanoma. N. Engl. J. Med. *363*, 2191–2199. https://doi.org/10.1056/NEJMoa1000584.
47. Schrenk, S., Bischoff, L.J., Goines, J., Cai, Y., Vemaraju, S., Odaka, Y., Good, S.R., Palumbo, J.S., Szabo, S., Reynaud, D., et al. (2023). MEK inhibition reduced vascular tumor growth and coagulopathy in a mouse model with hyperactive GNAQ. Nat. Commun. *14*, 1929. https://doi.org/10.1038/s41467-023-37516-7.
48. Langbroek, G.B., Stor, M.L.E., Janssen, V., de Haan, A., Horbach, S.E.R., Graupera, M., van Noesel, C.J.M., van der Horst, C.M.A.M., Wolkerstorfer, A., and Huveneers, S. (2024). Characterization of patient-derived GNAQ mutated endothelial cells from capillary malformations. J. Invest. Dermatol. *144*, 1378–1388.e1. https://doi.org/10.1016/j.jid.2023.10.033.
49. Khalili, J.S., Yu, X., Wang, J., Hayes, B.C., Davies, M.A., Lizee, G., Esmaeli, B., and Woodman, S.E. (2012). Combination small molecule MEK and PI3K inhibition enhances uveal melanoma cell death in a mutant GNAQ- and GNA11-dependent manner. Clin. Cancer Res. *18*, 4345–4355. https://doi.org/10.1158/1078-0432.CCR-11-3227.
50. Reed, K.E., Westphale, E.M., Larson, D.M., Wang, H.Z., Veenstra, R.D., and Beyer, E.C. (1993). Molecular cloning and functional expression of human connexin37, an endothelial cell gap junction protein. J. Clin. Invest. *91*, 997–1004. https://doi.org/10.1172/JCI116321.
51. Chen, K.H., Huang, H.Y., Chen, T.C., Liu, Y.J., Lin, I.C., Ng, K.F., Chuang, H.C., and Huang, S.C. (2022). A clinicopathological reappraisal of orbital vascular malformations and distinctive GJA4 mutation in cavernous venous malformations. Hum. Pathol. *130*, 79–87. https://doi.org/10.1016/j.humpath.2022.10.002.
52. Fang, J.S., and Burt, J.M. (2023). Connexin37 Regulates Cell Cycle in the Vasculature. J. Vasc. Res. *60*, 73–86. https://doi.org/10.1159/000525619.
53. Hamard, L., Santoro, T., Allagnat, F., Meda, P., Nardelli-Haefliger, D., Alonso, F., and Haefliger, J.A. (2020). Targeting connexin37 alters angiogenesis and arteriovenous differentiation in the developing mouse retina. Faseb. J. *34*, 8234–8249. https://doi.org/10.1096/fj.202000257R.
54. Gonzalez, L.F., Lekovic, G.P., Eschbacher, J., Coons, S., Porter, R.W., and Spetzler, R.F. (2006). Are cavernous sinus hemangiomas and cavernous malformations different entities? Neurosurg. Focus *21*, e6. https://doi.org/10.3171/foc.2006.21.1.7.
55. Cox, E.M., Bambakidis, N.C., and Cohen, M.L. (2017). Pathology of cavernous malformations. Handb. Clin. Neurol. *143*, 267–277. https://doi.org/10.1016/B978-0-444-63640-9.00025-4.
56. Li, Z.H., Wu, Z., Zhang, J.T., and Zhang, L.W. (2019). Surgical Management and Outcomes of Cavernous Sinus Hemangiomas: A Single-Institution Series of 47 Patients. World Neurosurg. *122*, e1181–e1194. https://doi.org/10.1016/j.wneu.2018.11.015.
57. Lee, C.C., Sheehan, J.P., Kano, H., Akpinar, B., Martinez-Alvarez, R., Martinez-Moreno, N., Guo, W.Y., Lunsford, L.D., and Liu, K.D. (2017). Gamma Knife radiosurgery for hemangioma of the cavernous sinus. J. Neurosurg. *126*, 1498–1505. https://doi.org/10.3171/2016.4.JNS152097.
58. Helmy, M., Liao, Y., Zhang, Y., and He, K. (2023). The Treatment Outcomes of Radiotherapy and Surgical Treatment for Patients with Cavernous Sinus Hemangioma: A Meta-Analysis. World Neurosurg. *178*, e345–e354. https://doi.org/10.1016/j.wneu.2023.07.068.
59. Chou, C.W., Wu, H.M., Huang, C.I., Chung, W.Y., Guo, W.Y., Shih, Y.H., Lee, L.S., and Pan, D.H.C. (2010). Gamma knife surgery for cavernous hemangiomas in the cavernous sinus. Neurosurgery *67*, 611–616. ; discussion 616. https://doi.org/10.1227/01.NEU.0000378026.23116.E6.
60. Matsui, Y., Mineharu, Y., Satow, T., Takebe, N., Takeuchi, E., and Saiki, M. (2014). Coexistence of multiple cavernous angiomas in the spinal cord and skin: a unique case of Cobb syndrome. J. Neurosurg. Spine *20*, 142–147. https://doi.org/10.3171/2013.11.SPINE13419.
61. Matsumaru, Y., Pongpech, S., Laothamas, J., Alvarez, H., Rodesch, G., and Lasjaunias, P. (1999). Multifocal and metameric spinal cord arteriovenous malformations. Review of 19 cases. Intervent Neuroradiol. *5*, 27–34. https://doi.org/10.1177/159101999900500105.
62. Sheppard, S.E., Sanders, V.R., Srinivasan, A., Finn, L.S., Adams, D., Elton, A., Amlie-Lefond, C., Nelson, Z., Dmyterko, V., Jensen, D., et al. (2021). Cerebrofacial vascular metameric syndrome is caused by somatic pathogenic variants in PIK3CA. Cold Spring Harb. Mol. Case Stud. *7*, a006147. https://doi.org/10.1101/mcs.a006147.
63. Jiarakongmun, P., Alvarez, A., Rodesch, G., and Lasjaunias, P. (2002). Clinical course and angioarchitecture of cerebrofacial arteriovenous metameric syndromes. Three demonstrative cases and literature review. Intervent Neuroradiol. *8*, 251–264. https://doi.org/10.1177/159101990200800305.
64. Bhattacharya, J.J., Luo, C.B., Suh, D.C., Alvarez, H., Rodesch, G., and Lasjaunias, P. (2001). Wyburn-Mason or Bonnet-Dechaume-Blanc as Cerebrofacial Arteriovenous Metameric Syndromes (CAMS). A New Concept and a New Classification. Intervent Neuroradiol. *7*, 5–17. https://doi.org/10.1177/159101990100700101.
65. Schmidt, A., Brixius, K., and Bloch, W. (2007). Endothelial precursor cell migration during vasculogenesis. Circ. Res. *101*, 125–136. https://doi.org/10.1161/CIRCRESAHA.107.148932.